Parachute Canopy Stress Measurements at Steady State and During Inflation

H. G. Heinrich*
University of Minnesota, Minneapolis, Minn.
and
David P. Saari†
FluiDyne Engineering Corporation, Minneapolis, Minn.

Circumferential stresses were measured on 5-ft flat circular block-constructed solid cloth and ringslot parachutes in a wind tunnel during inflation under infinite mass condition and at steady state. Five Omega senors placed along gore centerlines and a force link measured stresses and the parachute force versus time. Radial stresses were measured on a 3-ft solid flat circular block-constructed parachute at steady state. Stress measurements were evaluated in view of maximum and steady-state stresses versus location and time, as well as in respect to the parachute force. The measurements indicated strong stress variations, being different for both types of parachutes. In the 3-ft solid cloth parachute, the radial stress was, at certain locations, greater than the circumferential stress.

Nomenclature

D_0 = nominal diameter
F = parachute force
R_0 = $D_0/2$
S = distance from vent center
S^* = dimensionless distance $2S/D_0$
n = dimensionless factor
q = dynamic pressure
t = time
σ = stress, lb/ft
σ^* = normalized stress = σ/qD_0
$d\sigma/dt$ = stress rate
ϵ = strain
$d\epsilon/dt$ = strain rate

Subscripts

c = circumferential
LC = load cell, force indicator
r = radial
ss = steady state
m = maximum
Ω = Omega stress sensor

I. Introduction

A NUMBER of methods have been proposed to calculate the stress in parachutes under steady-state conditions and during inflation.[1-11] Many of the newer publications have certain features in common. For example, Refs. 6-9 assume that the cloth between the suspension lines bulges out in circular arcs; Refs. 6 and 11 also attempt to calculate a canopy profile based on the equilibrium between the aerodynamic forces and the static forces of the suspended load transmitted via the suspension lines; Refs. 7 and 8 utilize a canopy profile determined either from model or full-size tests. References 7 and 8 also propose a method of canopy stress calculation during the parachute inflation assuming canopy profiles consisting of truncated cones capped by hemispheres. Asfour[9] attempted to correlate an opening shock theory with inertial forces and stresses in the canopy. Saliaris[11] calculated circumferential as well as radial stresses. However, none of these theories has been confirmed experimentally.

Measurements of the stress in a flexible lightweight parachute canopy is difficult for a number of reasons. In solid cloth parachutes, the canopy stress is a biaxial problem, and most parachutes are also built under bias construction. Furthermore, the stress-strain characteristics of commonly used parachute cloths are nonlinear and vary with the stress rate $d\sigma/dt$. In addition, it has been mentioned repeatedly that any mechanical or electrical device attached to the canopy cloth interferes with the natural stress flux and that the stresses measured with such a device would not represent the true stresses in a parachute canopy. During inflation, the gores of a parachute canopy change considerably in profile and shape, and a stress sensor for the parachute cloth must be insensitive to the flexing of the cloth. Therefore, the usual stress measurement method of attaching a strain gage directly to the cloth or fastening a thin metal tab to the cloth and a strain gage to the tab gives erroneous results. In fact, it was shown that sensors of this type may also indicate compressive stress in the cloth.[12,13]

II. The Omega Sensor

In view of these problems, the Omega senor[12,13] shown in Fig. 1 was designed. Using a curved beam as the deforming element makes the sensor very sensitive. In order to avoid the transfer of bending moments resulting from the flexing of the canopy gores, it is attched to the parachute canopy by means of cloth tabs, which act as ideal hinges. The net effect of a possible interference with the natural stress flux is eliminated by means of calibration of the Omega sensor versus an applied stress after the sensor is attached to the parachute canopy. Utilizing such calibrations, satisfactory agreement was found between calculated and measured stress of a parachute canopy under steady-state conditions inflated in a wind tunnel.[12,13]

In view of the fact that the stress-strain characteristics of nylon, dacron, and other synthetic materials not only have a nonlinear stress-strain relationship, but that the stress-strain characteristics also depend on the strain rate, Omega senosrs were calibrated at various strain rates.[14] Figure 2 shows the

Presented as Paper 75-1374 at the AIAA 5th Aerodynamic Deceleration Systems Conference, Albuquerque, N. Mex., Nov. 17-19, 1975; submitted June 14, 1976; revision received Feb. 23, 1978.

Index categories: Deceleration Systems; Structural Design; Safety.
*Professor. Fellow AIAA.
†Development Engineer. Member AIAA.

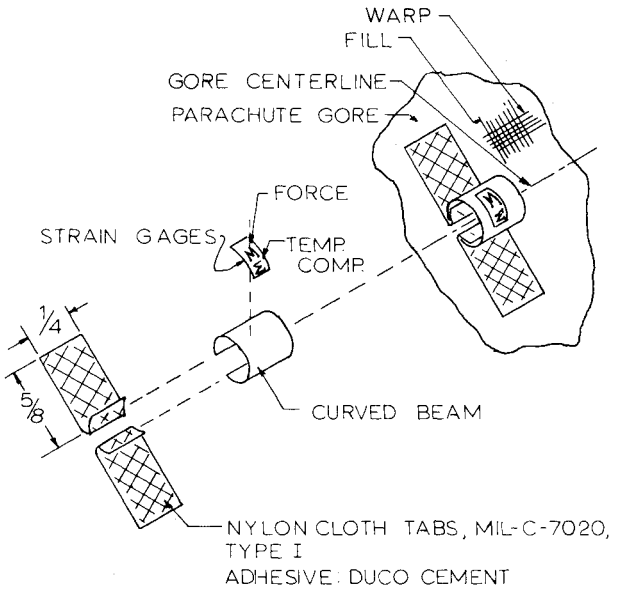

Fig. 1 Omega sensor.

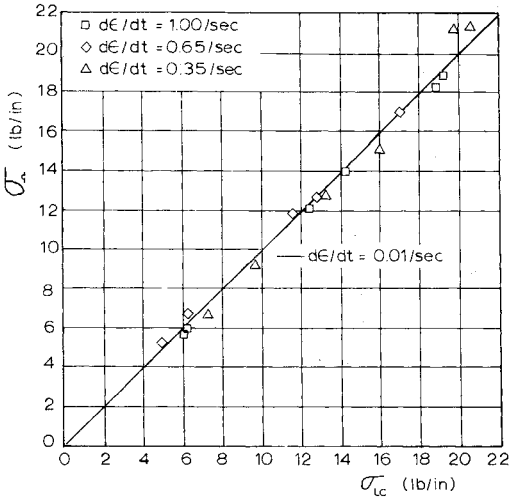

Fig. 2 Stresses measured by Omega sensor and load cell at strain rates of 0.35/s to 1.00/s.

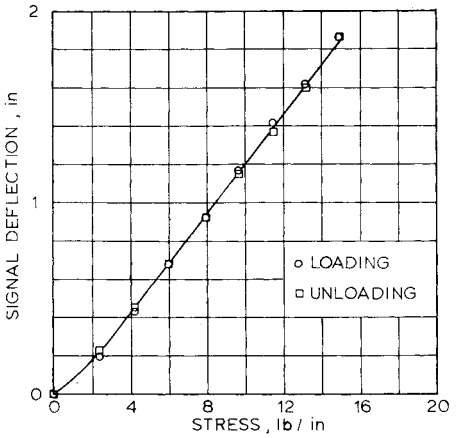

Fig. 3 Calibration of Omega sensor no. 14 fastened to parachute cloth Mil-C-7020 under biaxial loading (specimen VII).

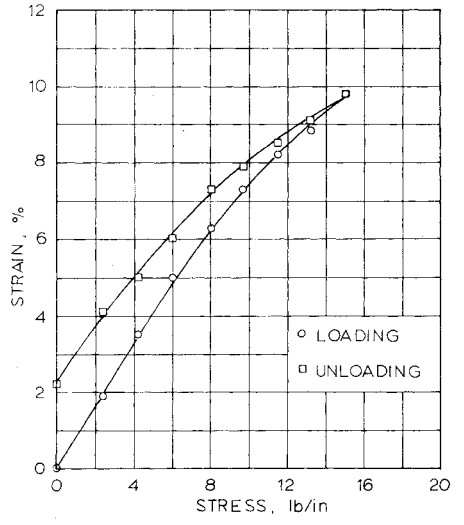

Fig. 4 Stress-strain behavior of parachute cloth Mil-C-7020 under biaxial loading (specimen VIII).

results of such a calibration. It can be seen that the calibration of the Omega sensor remain linear and independent of the rate of loading up to strain rates of 100% per second, $d\epsilon/dt = 1.0/s$. Also, there are no indications that the sensor would become rate sensitive at higher strain rates. The independence of the sensor output from the strain rate results because the Omega sensor does not measure strain of the cloth, which then is translated into stress, but actually measures the stress in the cloth directly.

Figures 3 and 4 show the Omega sensor output and the strain of a nylon specimen versus the applied stress for a biaxial loading and unloading cycle. One notices that the sensor output remains proportional to the applied stress, whereas the cloth strain varies considerably, showing strong hysteresis. This independence of the Omega sensor output from the cloth strain has been shown in many similar tests. Tests have also shown that the stress-strain and hysteresis characteristics of nylon cloth change after repeated loading cycles and that these characteristics are further altered when different recovery times are permitted. Since the Omega sensor is capable of measuring actual stresses independent of instantaneous strain and hysteresis effects and also maintains its linear calibration characteristic over a wide range of strain rates, it appeared justified to use this sensor for stress measurements on model parachute canopies at steady state and during inflation.

III. Radial and Circumferential Canopy Stress

In exploratory experiments, circumferential and radial stresses were measured on solid flat circular parachute models under steady-state conditions. Figure 5 shows normalized radial and circumferential stresses. It is interesting to note that at a location of approximately 0.75 R_0 the radial stress is greater than the circumferential stress. The radial stress vanishes toward the skirt of the parachute. Later tests showed that circumferential stress exists at the skirt. Unfortunately, only five measuring points along the gore centerline could be obtained, but the tests were repeatable, and, in the opinion of the authors, Fig. 5 is a valid indication of the actual stress distribution of solid cloth parachutes.

IV. Circumferential Stress During Inflation

Further exploratory stress measurements were made with 5-ft solid flat circular and flat 14% geometric porosity ringslot model parachutes during inflation and at steady state. The solid flat parachute had 28 gores, and the ringslot parachute had 32 gores and 64 vertical ribbons. The model geometries were similar to the standard C-9 solid flat circular parachute and the standard U.S. Air Force 32-ft ringslot parachute. Five Omega sensors were located at various positions on the gore centerlines of five different gores on each model in order to measure circumferential stresses.

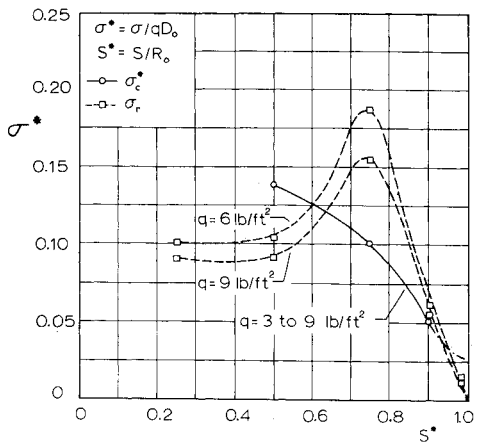

Fig. 5 Measured circumferential and radial stresses.

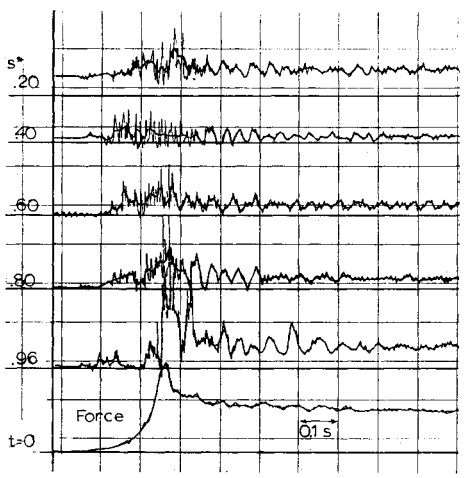

Fig. 6 Canopy stresses and total force of a solid flat circular model parachute, $q = 7.1$ psf (test 1).

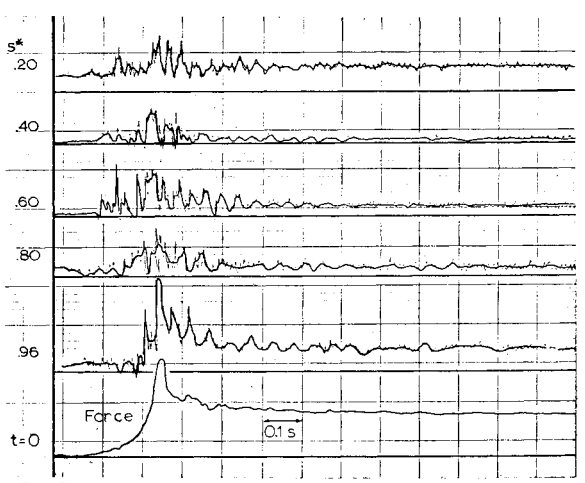

Fig. 7 Canopy stress and total force of a solid flat circular model parachute, $q = 7.1$ psf (test 5).

For the tests, the parachute models were enclosed in a metal container and suspended in a wind tunnel with stretched-out suspension lines. The desired wind velocity was then established and the container quickly removed. The suspension point of the parachute was fixed, and the inflation, therefore, occurred under infinite mass condition. Since the suspension lines were stretched out before removal of the container, the snatch force was eliminated. The instant of container removal was marked on the oscillogram, which recorded the Omega sensor and force link outputs.

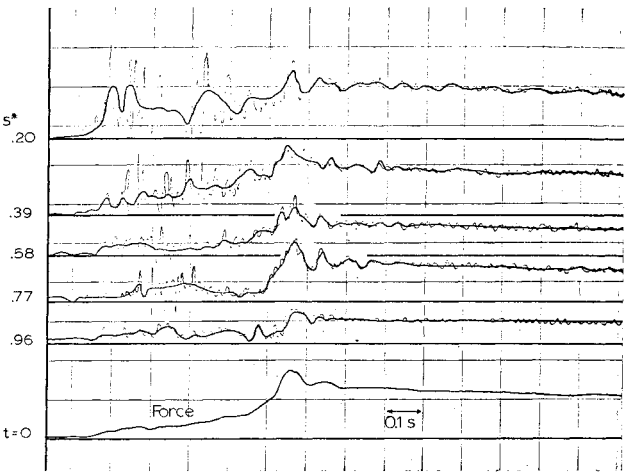

Fig. 8 Canopy stress and total force of a 32-gore ringslot model parachute, $q = 9.0$ psf (test 1)

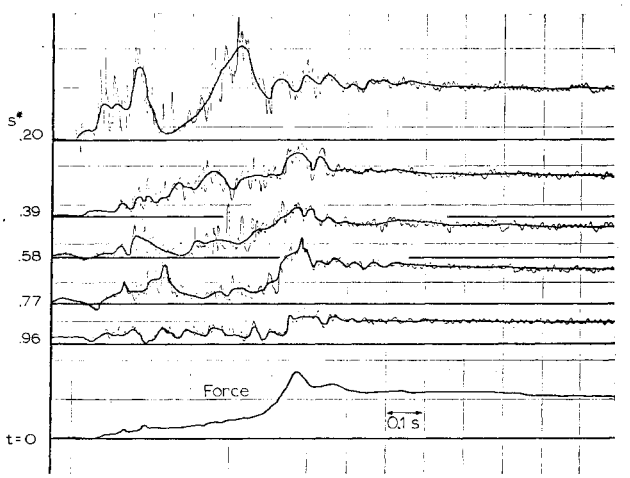

Fig. 9 Canopy stress and total force of a 32-gore ringslot model parachute, $q = 9.0$ psf (test 2).

Figures 6-9 show test diagrams of canopy stresses and forces versus time for the solid flat circular and ringslot model parachutes. A considerable number of experiments were made, and these diagrams are characteristic in view of stress and force levels, as well as stress and force variation with respect to time. Reviewing Figs. 6-9, one notices first of all the differences of the ratios of maximum to steady-state force of the solid flat and ringslot parachutes. This ratio is generally called the parachute "X factor." The level of the maximum stresses at the various locations along the gore centerlines is the next significant indication, and the diagrams of Figs. 6-9, as well as additional diagrams, were evaluated with respect to the maximum stress.

Figures 10 and 11 show the results of these evaluations. For easier comparison, the curve of Fig. 11 is transposed as a dashed line in Fig. 10. One notices a certain identity of the suggested curves, except that the normalized stresses of the solid flat circular parachute near the vent and near the skirt are considerably higher on the ringslot parachute. The dispersion of the data points shown in Figs. 10 and 11 is also interesting.

Figures 12 and 13 indicate the instant at which the maximum stresses occur in relationship to the time at which the total parachute force is at its maximum, $t_m/t_{F_m} = t_m{}^*$. This is of interest, since one may tend to believe that the maximum stress may occur when the parachute develops the maximum force. Reviewing Figs. 12 and 13, one notices that in the solid flat circular parachute the maximum stress at the various locations occurs somewhat before the instant of

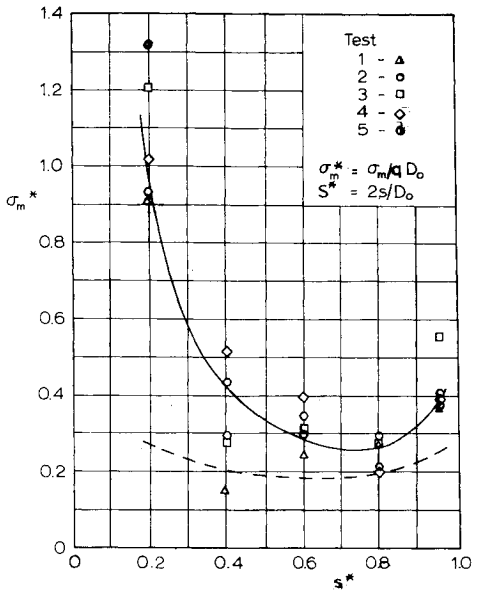

Fig. 10 Maximum stress $\sigma_m{}^*$ of the solid flat parachute, $q = 7.1$ psf (---ringslot parachute, Fig. 11).

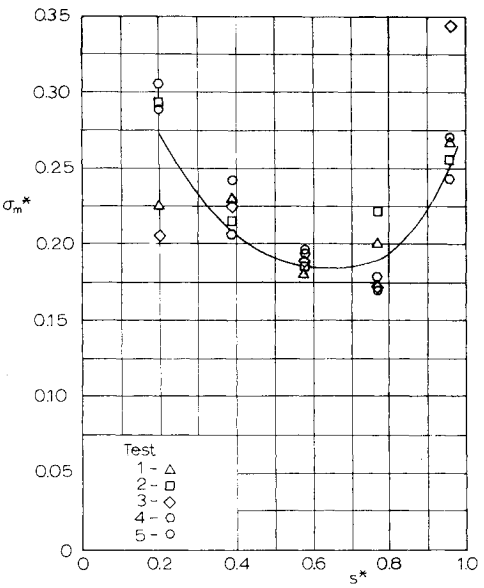

Fig. 11 Maximum stress $\sigma_m{}^*$ of the ringslot parachute, $q = 9.0$ psf.

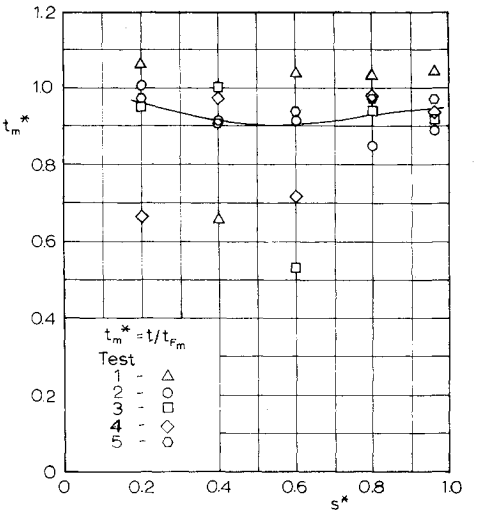

Fig. 12 Time of maximum stress $t_m{}^*$ of a solid flat parachute, $q = 7.1$ psf.

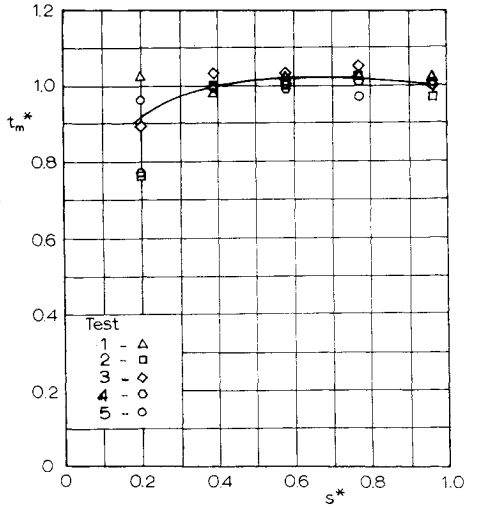

Fig. 13 Time of maximum stress $t_m{}^*$ of a ringslot parachute, $q = 9.0$ psf.

maximum force. On the ringslot parachute, the maximum stress in the vent region also occurs before the instant of maximum force, whereas in the middle section the maximum stress occurs later than the maximum force.

Figures 14 and 15 show the stresses at steady state and Figs. 16 and 17 the ratios of maximum to steady-state stress of the two types of parachutes. Again, for easier comparison, the curves for the ringslot parachute are transposed in the respective figures of the solid flat parachute. From Figs. 14 and 15, one notices that the steady-state stresses in the ringslot parachute are much more uniform throughout the canopy than those of the solid flat circular parachute. Also, the ratio of the maximum to the minimum stress of the ringslot parachute is lower and more evenly distributed than the corresponding ratio for the solid flat circular parachute (Figs. 16 and 17). In Fig. 16, one notices a large dispersion of the data points at $S^* = 0.4$. It appears that this sensor malfunctioned, and unfortunately this was detected only after the parachute was removed from the wind tunnel.

It was already shown that at various locations the maximum stress does not occur at the instant of the maximum parachute force. It is now also interesting to investigate whether the maximum stress is proportional to the maximum force. Asfour[9] pointed out that during the parachute inflation significant stresses may be developed due to inertial forces when the radial motion of the parachute cloth vanishes. In order to examine the maximum stress versus force relationship, one may write

$$\sigma_m/\sigma_{ss} = nF_m/F_{ss} \tag{1}$$

If the maximum stress is merely a function of parachute opening force, n would be unity. From the experiments, all terms of Eq. (1) are known, and one can find

$$n = (\sigma_m/\sigma_{ss})\,(F_{ss}/F_m) \tag{2}$$

Figures 18 and 19 show this relationship for both parachute models.

One notices that over a wide range, for both parachutes, the stress ratios are higher than the force ratios. It is unlikely that the stress measurements are falsely high due to strain rate sensitivity, since the maximum strain rates of the parachute cloth are estimated to be less than 0.6/s, well within the proven range for the Omega sensor. Therefore, the high n values seem to indicate that other factors besides the

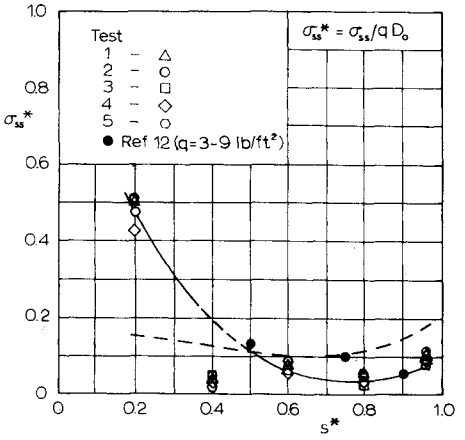

Fig. 14 Steady-state stress, $\sigma_{ss}{}^*$ of a solid flat parachute, $q = 7.1$ psf (---ringslot parachute, Fig. 15).

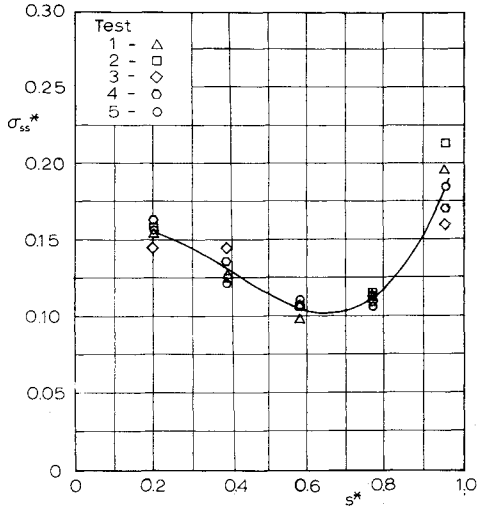

Fig. 15 Steady-state stress $\sigma_{ss}{}^*$ of a ringslot parachute, $q = 9.0$ psf.

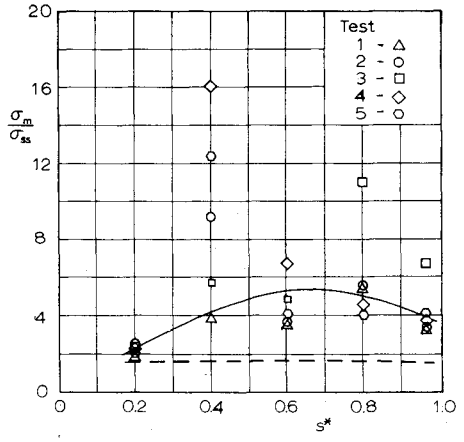

Fig. 16 Ratio of maximum and steady-state stresses of a solid flat parachute, $q = 7.1$ psf (---ringslot parachute, Fig. 17).

measured parachute force influence the stresses. For example, during inflation the bulge radii of the gores are probably larger than during steady state. Also, inertial forces will be developed in the gores when the rapid motion of the parachute cloth and suspension lines is retarded as the parachute approaches its maximum diameter. Furthermore, one may agree with Asfour[9] that there are significant stresses developed by the included air, which has an overall radial velocity component while the parachute inflates. This air movement must

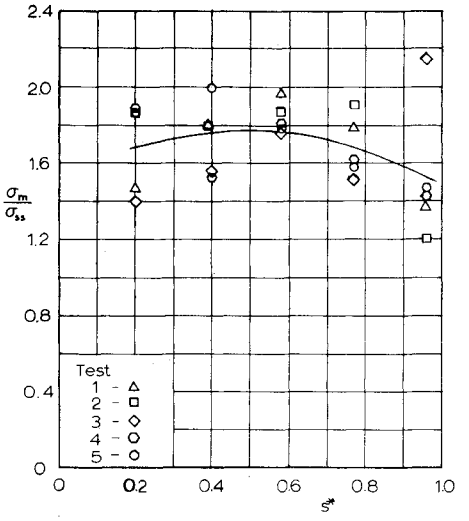

Fig. 17 Ratio of maximum and steady-state stresses of a ringslot parachute, $q = 9.0$ psf.

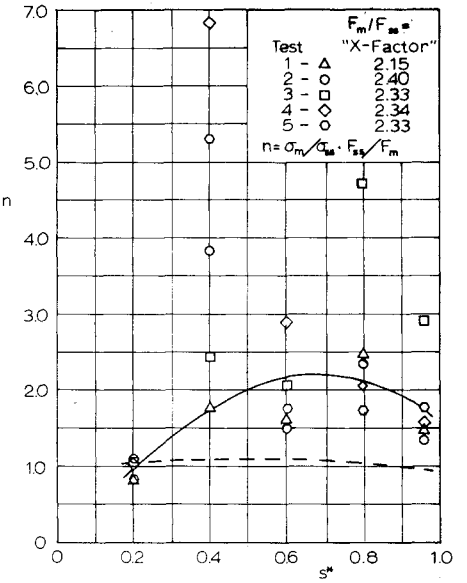

Fig. 18 Ratio of maximum stresses to steady-state stresses of a solid flat parachute under dynamic conditions (---ringslot parachute, Fig. 19).

also be retarded when the respective sections of the gore approach their final profile.

These and perhaps additional effects are reflected in the stress-time histories, causing the n value to differ from unity. The fact that the n values for the solid flat circular parachute are significantly higher than those of the ringslot parachute supports this speculation, because the opening time of the solid cloth parachute is shorter, and consequently the dynamic terms of the solid cloth parachute must be stronger than those of the ringslot parachute.

All recordings indicate that the stress in the two types of parachutes differs considerably in magnitude, distribution, and stress-time characteristics. However, it should also be kept in mind that the forces and stresses were measured under an infinite load inflation condition. The stress characteristics may differ when the parachutes inflate with finite loads.

V. Conclusion

The described stress measurements are exploratory. However, a number of measurements were made, and the tests were repeatable enough to have a certain degree of confidence in the results. The data points related to the solid

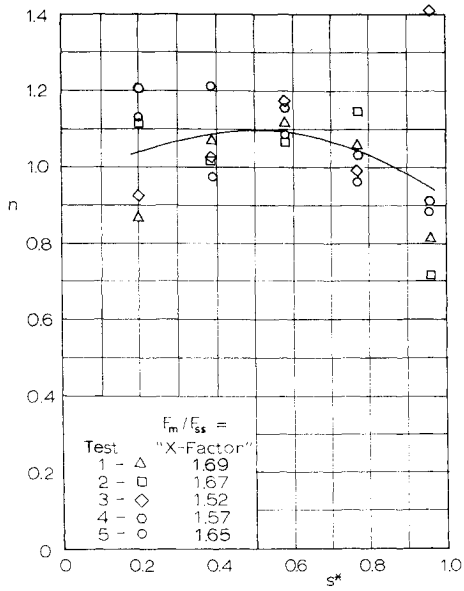

Fig. 19 Ratio of maximum stress to steady-state stresses of a ringslot parachute under dynamic conditions.

cloth parachute show a larger dispersion than those of the ringslot parachute. The degree of dispersion depends, of course, on uniformity of the parachute inflation, and it is known that the pattern of inflation of solid cloth models and full-size parachutes varies considerably. This nonuniformity is usually recognized by the wide variation of opening forces and opening times.[15-17]

An attempt to establish least-mean-square averages from the data failed because of an insufficient number of data points. Therefore, the indicated curves represent the best estimates of the authors. Also, at present only stress measurements on model parachutes are available. However, good model tests have, in the past, always given reasonable indications for conditions existing in prototype parachutes.

Based on the presented cahracteristics and considering the design details of the models, the following conclusions are drawn:

1) In block-constructed solid flat circular paracutes, the steady-state radial stress exceeds the circumferential stress at certain locations. During inflation and at steady state, the circumferential stress is highest at the vent region.

2) In ringslot parachutes, the stress is about equal at the vent and at the skirt during inflation; under steady state, the stress is higher at the skirt than at the vent.

3) Both types of parachutes have low levels of circumferential stress at the middle section of the canopy during inflation and at steady state. During inflation, the general stress level of ringslot parachutes is considerably lower than that of the solid cloth parachute.

4) During inflation, the maximum stresses in both types of parachutes does not necessarily occur at the instant of maximum parachute force.

5) There are indications that during inflation a varying gore geometry and dynamic forces contribute significantly to the development of stresses in a parachute canopy. These effects are stronger on the solid cloth than on the ringslot parachute.

Acknowledgment

The study was sponsored by the U.S. Air Force Contracts F33615-68-C-1227, F33615-73-R-3149, and F33615-C-0020 and funds from the University of Minnesota.

References

[1] Jones, R., "On the Aerodynamic Characteristics of Parachutes," Aeronautical Research Committee, R. & M. 862, His Majesty's Stationery Office, London, England, June 1923.

[2] Stevens, G. W. H. and Johns, T. F., "The Theory of Parachutes with Cords over the Canopy," Ministry of Supply, Aeronautical Research Council, R. & M., His Majesty's Stationery Office, London, England, 1949.

[3] Duncan, W. J., Stevens, G. W. H., and Richards, G. J., "Theory of the Flat Elastic Parachute," Ministry of Supply, Aeronautical Research Council, R. & M. 2118, His Majesty's Stationery Office, London, England, 1942.

[4] Beck, E., "The Parachute Considered as a Flexible Shell of Rotation," U.S. Air Force Transl. F-TS-3630-Re-BR-281, Nov. 1942.

[5] Reagan, J. F., "A Theoretical Investigation into the Dynamics and Stress Analysis of Parachutes for the Purpose of Determining Design Factors," Daniel Guggenheim Airship Inst., Rept. 130, Feb. 1945.

[6] Topping, A. D., Marketos, J. D., and Costakos, N. C., "A Study of Canopy Shapes and Stresses for Parachutes in Steady Descent," Goodyear Aircraft Corp., WADC TR 55-294, Oct. 1955.

[7] Heinrich, H. G. and Jamison, L. R., "Stress Analysis of a Parachute During Inflation and at Steady State," Air Force Flight Dynamics Lab., FDL-TDR-64-125. Feb. 1965.

[8] Heinrich, J. G. and Jamison, L. R. Jr., "Parachute Stress Analysis during Inflation and at Steady State, " *Journal of Aircraft,* Vol. 3, Jan.-Feb. 1966, pp. 52-58.

[9] Asfour, K. F., "Analysis of Dynamic Stress in an Inflating Parachute," *Journal of Aircraft,* Vol. 4, Sept.-Oct. 1967, pp. 429-433.

[10] Ross, E. W. Jr., "Approximate Analysis of a Flat, Circular Parachute in Steady Descent," U.S. Army Natick Lab., TR 69-51-OSD, Dec. 1968.

[11] Saliaris, C., "Angenaeherte Berechnung der Kraefte, Spannungen und Form des ebenen Rundkappenfallshirms im gefuellten Zustand," Deutsche Forschungs- und Versuchsanstalt fuer Luft- und Raumfahrt Institut fuer Flugmechanik, Braunschweig, Germany, Forschungsbericht 71-98, Aug. 1971.

[12] Heinrich, H. G. and Noreen, R. A., "Stress Measurements on Inflated Model Parachutes," Air Force Flight Dynamics Lab. AFFDL-TR-72-43, Feb. 1972.

[13] Heinrich, H. G. and Noreen, R. A., "Experimental Stress Analysis on Inflated Model Parachutes," *AIAA 4th Aerodynamic Deceleration Systems Conference,* Palm Springs, Calif., May 21-23, 1973.

[14] Heinrich, H. G. and Noreen, R. A., "Functioning of the Omega Sensor on Textile Samples under High Loading Rates," Air Force Flight Dynamics Lab., AFFDL-TR-74-78, Sept. 1974.

[15] Heinrich, H. G. and Hektner, T. R., "Flexibility as a Model Parachute Performance Parameter," *Journal of Aircraft,* Vol. 8, Sept. 1971, pp. 704-709.

[16] Heinrich, H. G. and Niccum, R. J., "A Method to Reduce Parachute Inflation Time with a Minor Increase of Opening Force," U.S. Air Force, WADD TR 60-761, Aug. 1960.

[17] Heinrich, H. G., "A Linearized Theory of Parachute Opening Dynamics," *The Aeronautical Journal,* Vol. 76, Dec. 1972, pp. 723-730.